Density Functional Theory Study of the Direct Conversion of Methane to Acetic Acid by $RhCl_3$

Iordan H. Hristov and Tom Ziegler*

Department of Chemistry, University of Calgary, 2500 University Drive NW, Calgary, Alberta, Canada T2N 1N4

Received March 21, 2003

It has recently been reported by Sen et al. that dioxygen can functionalize methane directly at low temperatures with $RhCl_3$ as the catalyst and I^- as the promoter. The main products are acetic acid and methanol, with formic acid as a side product. The active form of the catalyst is considered to be $[Rh(CO)_2I_2]^-$. We propose here a mechanism for the Sen process and investigated it theoretically with DFT. The proposed mechanism is as follows. In the first step, a methane C−H bond is activated by $[Rh(CO)_2I_2]^-$ either through an oxidative-addition process or by a σ-bond metathesis mechanism, leading in both cases to a $Rh-CH_3$ complex (**a**). In the next step a facile insertion of CO into the $Rh-CH_3$ bond leads to a $Rh-COCH_3$ complex (**b**). Finally, the hydrolysis of **a** and **b** produces methanol and acetic acid, respectively, and forms $[Rh(CO)_2IH]^-$ (**c**). The oxidation of **c** by O_2 leads to the peroxo complex $[(HOO)Rh(CO)_2I]^-$, which can react with another **c** to yield two hydroxo complexes of the form $[(HO)Rh(CO)_2I]^-$. Substitution of OH^- by I^- finally regenerates the $[Rh(CO)_2I_2]^-$ catalyst.

Introduction

Methane is the major constituent of natural gas, which is an abundant and inexpensive natural resource. Two of the highest volume functionalized organic commodities today are methanol and acetic acid, which are produced in quantities that amount to millions of tons in the USA alone.[1] The existing technology for conversion of methane to these products consists in all cases of a multistep process: (a) the high-temperature steam re-forming of alkanes to a mixture of $CO + H_2$ (syngas),[2] (b) high-temperature conversion of syngas to methanol,[3] and (c) carbonylation of methanol to acetic acid through the "Monsanto process".[4] A low-temperature "one pot" process for the direct oxidation of methane would be a very attractive alternative.

Rhodium is the third metal after platinum and iridium that has been used successfully to catalyze an isotopic hydrogen exchange. The rhodium catalyst first employed was $RhCl_3$ in a 1:1 mixture of acetic acid and water. This catalyst was active toward exchange of hydrogen in aromatic compounds.[5] The heterogeneous species produced upon reduction of the catalyst also exhibited catalytic activity.

Recently it was shown by Sen et al.[6] that the $[Rh(CO)_2I_2]^-$ complex used in the Monsanto process can catalyze the activation of C−H bonds in methane, as well as the oxidation of CH_4 by dioxygen to methanol and the carbonylation of methane to acetic acid. We shall study the same catalytic system in the present investigation. The solvent that was used experimentally was a 6:1 mixture of heptafluorobutyric acid and water at 80 °C with KI applied as promotor. The reactants are CH_4, CO, and O_2 at high pressure, and they are all necessary for the process.

The catalyst is introduced as $RhCl_3$, which under the reaction conditions is reduced to form the $[Rh(CO)_2I_2]^-$ catalytic species. This rhodium complex is also the catalyst in the water-gas shift reaction:[7]

$$H_2O + CO \rightarrow H_2 + CO_2 \quad (1)$$

However, in the experiments by Sen et al. the production of CO_2 was not observed.

Labeling experiments with C^{13} revealed the following relationship between reagents and products:

$$*CH_4 \rightarrow *CH_3OH, *CH_3COOH, H*COOH \quad (2)$$

$$*CH_3OH \rightarrow H*COOH \quad (3)$$

$$*CO \rightarrow H*COOH \quad (4)$$

One striking aspect of the process is that, although the reaction systems contain the same catalyst and reagents as in the Monsanto process, methanol is not carbonylated but oxidized to formic acid, which is only a minor side product.

(1) *Chem. Eng. News* **1996**, 40 (June 24).
(2) (a) *An Ulman's Encyclopedia: Industrial Inorganic Chemicals and Products*; Wiley-VCH: New York, 1999; Vol. 3, p 2446. (b) Cheng, W. H., Kung, H. H., Eds. *Methanol Production and Use*; Marcel Dekker: New York, 1994.
(3) (a) Stilles, A. B. *Catalyst Manufacture*; Marcel Dekker: New York, 1983; Vol. 3, p 125. (b) Zardi, U. *Hydrocarbon Process.* **1982**, *61*(8), 129. (c) Klier, K. *Adv. Catal.* **1982**, *31*, 243. (d) Supp, E. *Hydrocarbon Process.* **1981**, *60*(3), 71. (e) Kung, H. H. *Catal. Rev. Sci. Eng.* **1980**, *22*, 235 (e) Reference 2b.
(4) Forster, D. *Adv. Organomet. Chem.* **1979**, *17*, 255.
(5) Blake, M. R.; Garnett, J. L.; Gregor, I. K.; Hannan, W.; Hoa, K.; Long, M. A. *J. Chem. Soc., Chem. Commun.* **1975**, 930.
(6) (a) Lin, M.; Sen, A. *Nature* **1994**, *368*, 613. (b) Lin, M.; Hogan, T. E.; Sen, A. *J. Am. Chem. Soc.* **1996**, *118*, 4574.
(7) Baker, E. C.; Hendriksen, D. E.; Eisenber, R. *J. Am. Chem. Soc.* **1980**, *102*(3), 1020.

10.1021/om030217c CCC: $25.00
Publication on Web 07/25/2003

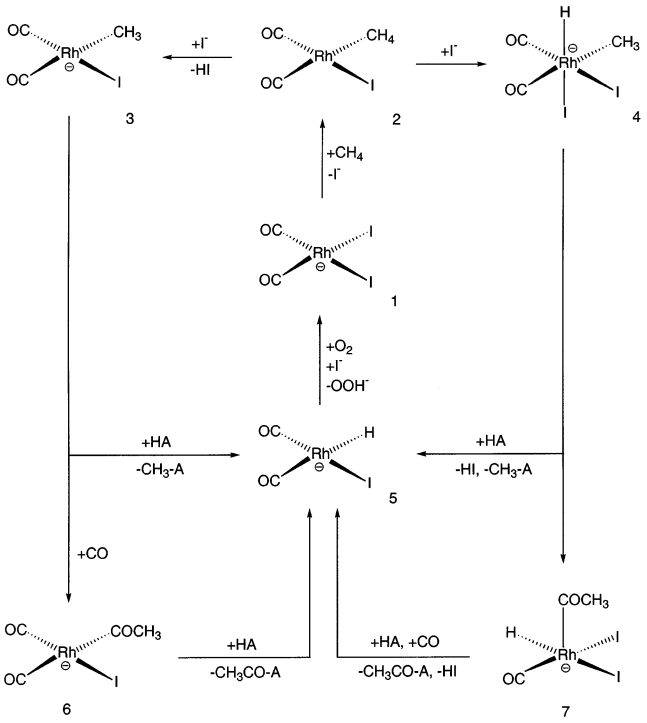

Figure 1. Proposed catalytic cycle for the Sen reaction.

The solvent was found to affect both the product ratio and the turnover rates, and it was chosen to maximize the rate of the reaction. Increasing the acid in the mixture resulted in higher turnover rates and higher selectivity toward methanol production.

We propose here a possible catalytic cycle for the process discovered by Sen et al., as outlined in Figure 1. In the proposed cycle methane forms first the σ-complex **2** with the $[Rh(CO)_2I_2]^-$ catalyst **1**, either through a dissociative mechanism where iodide is lost to produce a highly reactive tricoordinate species or, alternatively, through an associative S_N2 substitution mechanism. The methane complex **2** can in the next step undergo a metathesis reaction to produce the Rh^I-CH_3 complex **3** or an oxidative addition to form the Rh(III) hydride methyl complex **4** (Figure 1).

The methylated rhodium complexes **3** and **4** can subsequently undergo insertion of CO into the $Rh-CH_3$ bond to produce the acyl complexes **6** and **7**, respectively. Finally, CH_3COA is eliminated by the nucleophilic attack of heptafluorobutyric anion A^- on **6** and **7**, leading to the hydrido complex **5**, seen in Figure 1. Alternatively, the hydrido complex **5** could be formed by a nucleophilic attack of A^- on the methyl group in **3** or **4**, leading to CH_3A. Methanol and acetic acid are produced by hydrolysis of CH_3A and CH_3COA, respectively.

In the end, complex **5** is oxidized by O_2 to a peroxo complex, which could act as an oxidizing agent for **5**, thus producing 2 equiv of a Rh(I) hydroxy complex. Upon exchange of the OH^- ligands for I^- the $[Rh(CO)_2I_2]^-$ catalyst is regenerated. Another possible alternative is a direct substitution of the peroxo group in the complexes for I^- from the solution. We shall in the following probe the feasibility of the different steps proposed in this mechanism.

Computational Details

All DFT calculations were carried out using the Amsterdam Density Functional (ADF 2.3.3) program[8a] developed by Baerends et al.[8b] and vectorized by Ravenek.[8c] The numerical integration scheme applied for the calculations was developed by te Velde et al.[8d,e] The geometry optimization procedure was based on the Versluis and Ziegler[8f] method. Geometry optimizations were carried out and energy differences determined using the local density approximation of Vosko, Wilk, and Nusair (LDA VWN)[8g] augumented with the nonlocal gradient correction PW91 from Perdew and Wang.[8h] Relativistic corrections were added using a scalar-relativistic Pauli Hamiltonian.[8i] The electronic configurations of the molecular systems were described by a triple-ζ basis set for all atoms. Nonhydrogen atoms were assigned a relativistic frozen-core potential including 4p for I and Rh and 1s for C and O. A set of auxiliary s, p, d, and f functions, centered on all nuclei, was used to fit the molecular density and to represent the Coulomb and exchange potentials accurately in each SCF cycle. Transition states were located from a linear transit scan in which the reaction coordinate was kept fixed at different distances while all other degrees of freedom were optimized. After the linear transit search a transition state optimization procedure was employed to produce the transition states.

Solvation energies were calculated from gas-phase structures by using the conductor-like screening model (COSMO)[8j] that has been implemented recently into the ADF program.[8k] The solvation calculations were performed with a dielectric constant of 8.42 for trifluoroacetic acid.[8l] The radii used for the atoms (in Å) are as follows: H, 1.16; C, 2.3; O, 1.3; Rh, 1.35; I, 2.2; F, 1.33. Some of these values were obtained previously by optimization using least-squares fitting to experimental solvation energies.[8m] For the purposes of calculating the solvation entropies, the solvation process was broken into three steps, following Wertz.[8n,o] The gas-phase entropies $S°$ were calculated by standard methods based on statistical methods.[8p]

The COSMO method is not able to treat solvated halides accurately. Thus, the COSMO method underestimates the solvation energy of I^- by about 19.2 kcal/mol. We have for this reason in our calculations used the experimental values[8q] of $\Delta H_{solv}(I^-) = -71.8$ kcal/mol and $\Delta S_{solv}(I^-) = -11.2$. Detailed structural data are available as Supporting Information.

Results and Discussion

Structure of the Catalyst. We shall in the following provide a detailed discussion of the steps proposed in Figure 1 for the oxidation by O_2 of CH_4 to acetic acid (and methanol) with $[Rh(CO)_2I_2]^-$ as the catalyst.

(8) (a) Amsterdam Density Functional program, Division of Theoretical Chemistry, Vrije Universiteit, De Boelelaan 1083, 1081 HV Amsterdam, The Netherlands; www.scm.com. (b) Baerends, E. J.; Ellis, D. E.; Ros, P. *Chem. Phys.* **1973**, *2*, 41, 52. (c) Ravenek, W. In *Algorithms and Applications on Vector and Parallel Computers*; te Riele, H. J. J., Dekker, T. J., van de Horst, H. A., Eds.; Elsevier: Amsterdam, The Netherlands, 1987. (d) Boerrigter, P. M.; te Velde, G.; Baerends, E. J. *J. Comput. Chem.* **1988**, *33*, 87. te Velde, G.; Baerends, E. J. *J. Comput. Chem.* **1992**, *99*, 84. (e) te Velde, G.; Baerends, E. J. *J. Comput. Chem.* **1992**, *99*, 84. (f) Versluis, L.; Ziegler, T. *J. Chem. Phys.* **1988**, *88*, 322. (g) Vosko, S. H.; Wilk, L.; Nusair, M. *Can. J. Phys.* **1980**, *58*, 1200. (h) Perdew, J. P.; Chevary, J. A.; Vosko, S. H.; Jackson, K. A.; Pederson, M. R.; Singh, D. J.; Fiolhais, C. *Phys. Rev. B* **1992**, *46*, 6671. (i) Sinjders, J. G.; Baerends, E. J.; Ros, P. *Mol. Phys.* **1979**, *38*, 1909. (j) Klamt, A.; Schuurmann, G. *J. Chem. Soc., Perkin Trans. 2* **1993**, 799. (k) Rye, C. C.; Ziegler, T. *Theor. Chem. Acta* **1999**, *101*, 396. (l) Weast, R. C., Ed. *CRC Handbook of Chemistry and Physics*; CRC Press: Cleveland, OH, 1972. (m) Marcus, Y. *J. Chem. Soc., Faraday Trans.* **1991**, *87*(18), 2995 (n) Wertz, D. H. *J. Am. Chem. Soc.* **1980**, *102*, 5316. (o) Cooper, J.; Ziegler, T. *Inorg. Chem.* **2002**, *41*, 6614. (p) McQuarrie, D. A. *Statistical Thermodynamics*; Harper: New York, 1973. (q) Marcus, Y., *Ion Solvation*; Wiley: Chichester, U.K., 1985; pp 108, 126.

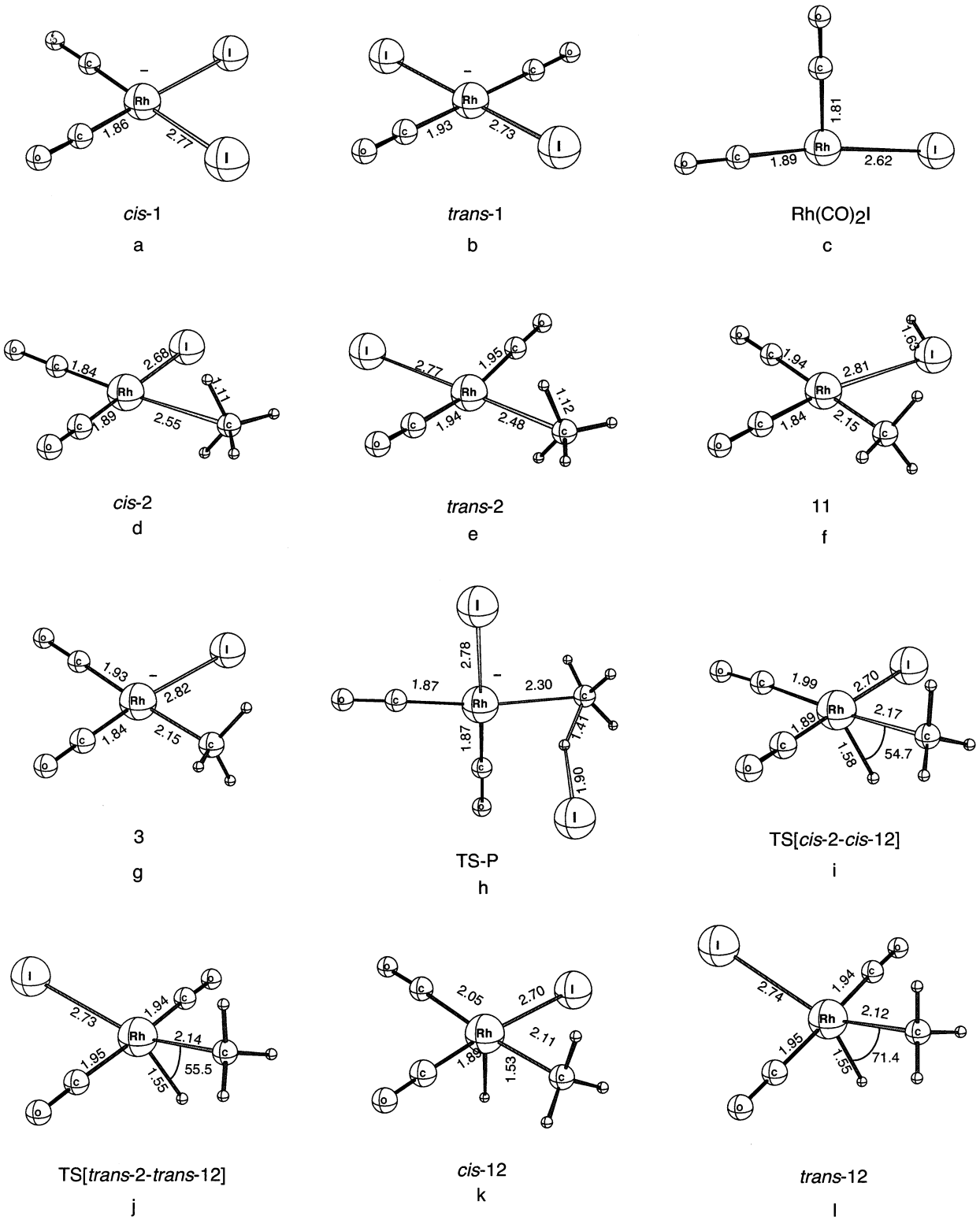

Figure 2. Optimized structures for the species involved in catalyst formation and C−H activation.

The $[Rh(CO)_2I_2]^-$ catalyst has a square-planar geometry with a d^8 low-spin configuration. The structure with CO and iodide in cis positions was preferred over the corresponding trans isomer by $\Delta G_{gas} = 9.7$ kcal/mol in the gas phase, as one would expect from the stronger trans-directing effect of the CO ligand and the facile donation of π-electrons from iodide to CO. The energy difference is enhanced slightly in solution to $\Delta G_{sol} = 11.3$ kcal/mol, due to the net dipole moment on the cis isomer. The structures for the cis and trans isomers are shown in parts a and b of Figure 2, respectively.

Formation of the Methane Complex. The energies for the uptake of methane and the formation of **2** are given in Table 1.

The substitution of one of the I^- ligands in **1** leads to the methane compound **2**, which is the starting complex for C−H activation. The substitution can take place either by a concerted nucleophilic S_N2 mechanism or,

Table 1. Energies[a,b] for Catalyst Formation and Methane Uptake

reacn	ΔH_{gas}	ΔS_{gas}	ΔG_{gas}	ΔH_{sol}[c]	ΔS_{sol}	ΔG_{sol}
cis-**1** + $H_2O \rightarrow$ *cis*-[$Rh(CO)_2I(H_2O)$] + I^-	30.9	−10.6	34.8	−7.4	−5.0	−5.6
cis-**1** + $CH_4 \rightarrow$ *cis*-**2** + I^-	44.5	11.7	40.4	6.3	−4.2	7.8
cis-**1** $\rightarrow$ [$Rh(CO)_2$|] + I^-	49.5	24.6	40.8	2.0	11.1	−1.9
[$Rh(CO)_2I$] + $CH_4 \rightarrow$ *cis*-**2**	−5.0	−33.9	7.0	4.3	−15.3	9.7

[a] ΔH and ΔG in kcal/mol at 353.16 K and 1 atm, in the solution (ΔH_{sol}, ΔG_{sol}) and gas phases (ΔH_{gas}, ΔG_{gas}). [b] ΔS in cal/(mol K) at 353.16 K and 1 atm, in the solution (ΔS_{sol}) and gas phases (ΔS_{gas}). $\Delta S_{sol} = \Delta S_{gas} + \Delta S_{solv}$. [c] $\Delta H_{sol} = \Delta H_{gas} + \Delta E_{el,sol}$. Here ΔE_{sol} is the electrostatic solvation energy from a COSMO calculation.[8f]

alternatively, through a dissociative mechanism where methane reacts with a tricoordinated $Rh(CO)_2I$ complex (Figure 2c) produced upon dissociation of one iodide ligand. Although very reactive, tricoordinated 14-electron complexes similar to [$Rh(CO)_2I$] have been isolated when bulky phosphine ligands are used instead of CO. These complexes easily associate neutral molecules: for example, N_2 and SO_2.[9] The [$Rh(CO)_2I$] complex does not form the dimer in aqueous solutions where the aqua complex [$Rh(CO)_2I(H_2O)$] is more stable. When aqueous HI is used instead to dissolve the dimer, the $[Rh(CO)_2I_2]^-$ species were in equilibrium with the aqua complex.[10] The aqua complex is more stable by $\Delta G = -5.6$ kcal/mol, and it will be the prevailing species. For the ligand exchange with methane, however, the less stable $[Rh(CO)_2I_2]^-$ complex will be more active, which can account for the 2-fold excess of KI that Sen used in his experiments which favors the formation of this diiodo complex.

In the dissociative mechanism one would have

$$\underset{\mathbf{1}}{\textit{cis}\text{-}[Rh(CO)_2I_2]^-} \rightarrow [Rh(CO)_2I] + I^- \qquad (5)$$

$$[Rh(CO)_2I] + CH_4 \rightarrow \underset{\mathbf{2}}{\textit{cis}\text{-}[Rh(CO)_2I(CH_4)]} \qquad (6)$$

with $G_5 = -1.9$ kcal/mol and $G_6 = 9.7$ kcal/mol in solution. These values can be understood if one considers entropy and solvation effects. Thus, the high solvation energy of I^- and the increase in entropy make the iodide dissociation (eq 5) favorable. On the other hand, the solvation energy of complex **2** is only 1.9 kcal/mol, whereas for the tricoordinated neutral complex [$Rh(CO)_2I$] the solvation energy is 12.3 kcal/mol. This is why the association reaction in eq 6 is endothermic in solution. In the gas phase it is slightly exothermic with $H_{gas} = -5$ kcal/mol. However, the CH_4 uptake in eq 6 is endoergonic in the gas phase as well as in solution due to the loss in entropy.

We also looked at a concerted nucleophilic substitution mechanism for the ligand exchange reaction. The transition state we obtained, however, corresponds to a complete dissociation of the ioidide ligand. Therefore, this mechanism converges to the dissociative mechanism for the exchange reaction.

The more likely mechanism, therefore, is the two-step dissociative ligand exchange mechanism. The overall reaction for the most stable cis isomers is

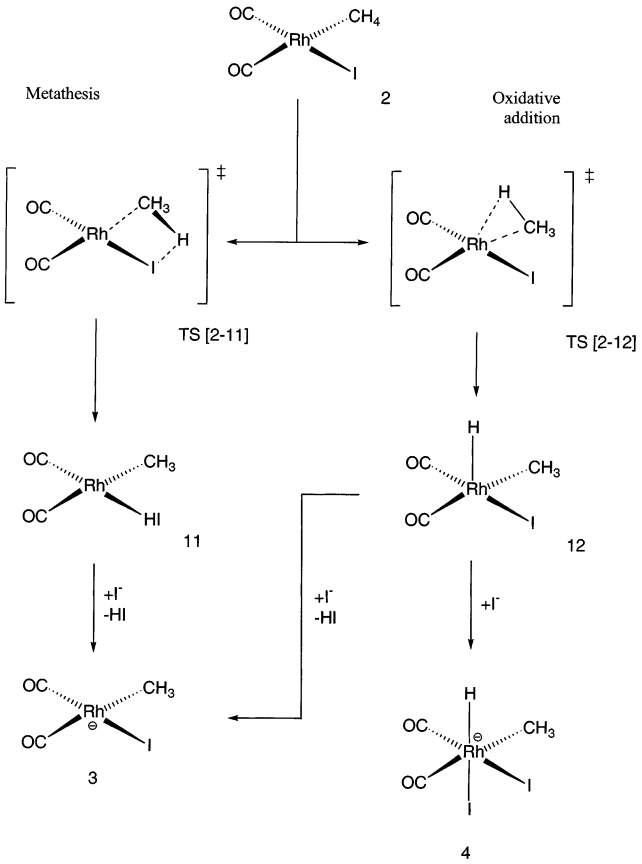

Figure 3. Metathesis and oxidative-addition mechanisms for the C−H activation step in the cis isomers.

$$\underset{\mathbf{1}}{\textit{cis}\text{-}[Rh(CO)_2I_2]^-} + CH_4 \rightarrow \underset{\mathbf{2}}{\textit{cis}\text{-}[Rh(CO)_2I(CH_4)]} + I^- \qquad (7)$$

with $G_7 = 7.8$ kcal/mol in solution.

The preferred conformation for both *cis*- and *trans*-[$Rh(CO)_2I(CH_4)$] is the η^2 isomer (Figure 2d,e). Here the elongated C−H bonds involved in bonding with the metal form a plane normal to the plane of the complex. Thus, these bonds are well-positioned for the oxidative-addition step in the subsequent C−H activation (**2** → **4**) of Figure 1. For the cis isomer the alternative mechanism for the C−H activation would be a metathesis reaction involving CH_4 and the neighboring iodine atom (**2** → **11** of Figure 3). The reaction steps in the C−H activation path for the cis isomers are shown in Figure 3.

C−H Activation by Metathesis. The energies for the C−H activation are given in Table 2, with the energy profile shown in Scheme 1.

For the metathesis mechanism (**2** → **11** of Figure 3) we find the reaction only to have a thermodynamical

(9) *Encyclopedia of Inorganic Chemistry*; Wiley: Chichester, U.K., 1994; Vol. 7, p 3471.
(10) Garlaschelli, L.; Marchionna, M.; Iapalucci, M. C.; Longoni, G. *J. Organomet. Chem.* **1989**, *378*, 457.

Scheme 1. Free Energy Profile for C−H Activation (kcal/mol)

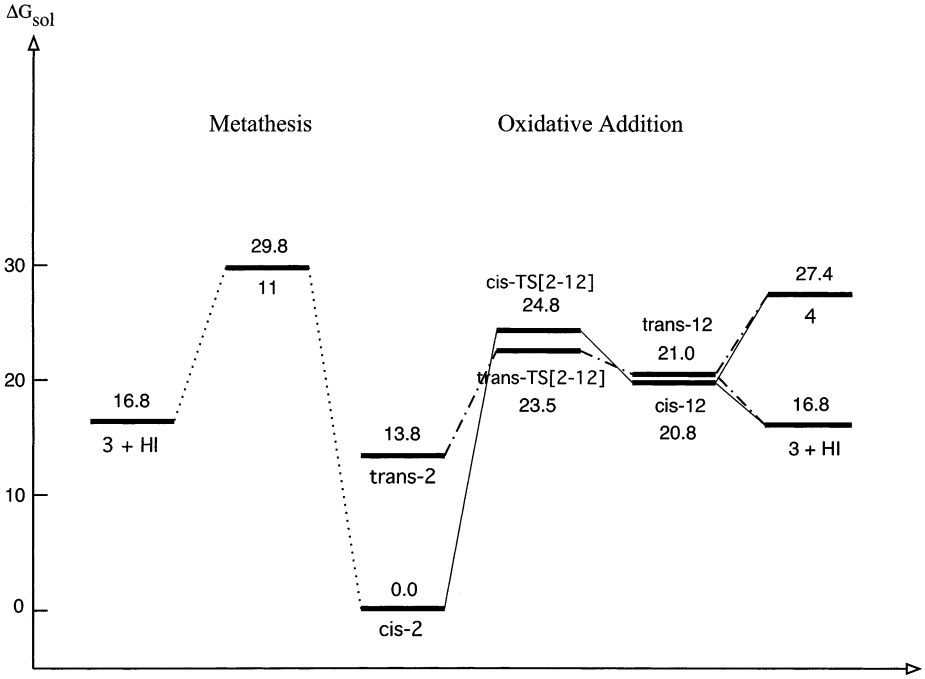

Table 2. Energies[a,b] for Metathesis and C−H Activation

reacn	ΔH_{gas}	ΔS_{gas}	ΔG_{gas}	ΔH_{sol}[c]	ΔS_{sol}	ΔG_{sol}
cis-**2** + I^- → **3** + HI	0.9	8.1	−2.0	18.1	3.7	16.8
cis-**2** + I^- → **4**	−14.2	−29.4	−3.8	22.7	−13.3	27.4
cis-**2** → **11**	31.8	3.5	30.6	30.4	1.6	29.8
11 + I^- → **3** + HI	−30.9	4.6	−32.6	−12.3	2.1	−13.0
cis-**2** → *cis*-TS[**2-12**]	23.8	−3.6	25.1	24.2	−1.7	24.8
cis-**2** → *cis*-**12**	21.7	1.2	21.2	21.0	0.6	20.8
cis-**2** → *trans*-**2**	11.8	−5.6	13.8	12.9	−2.6	13.8
cis-**12** + I^- → **3** + HI	−20.8	6.9	−23.2	−3.0	3.2	−4.1
cis-**12** + I^- → **4**	−35.8	−30.6	−25.0	1.7	−13.8	6.6
trans-**2** → *trans*-TS[**2-12**]	10.5	0.0	10.5	9.7	0.0	9.7
trans-**2** → *trans*-**12**	8.7	6.3	6.5	8.2	2.9	7.2
trans-**12** + I^- → **3** + HI	−19.6	−7.4	−22.3	−3.0	3.4	−4.2
trans-**12** + I^- → **4**	−34.7	−30.1	−24.1	1.6	−13.6	6.4

[a] See footnote *a* in Table 1. [b] See footnote *b* in Table 1. [c] See footnote *c* in Table 1.

barrier, so that the transition state indicated in Figure 3 as TS[**2-11**] actually does not exist. The structure with the highest energy was the $[Rh(CO)_2(HI)(CH_3)]$ complex **11** (Figure 2f), for which an unconstrained optimization was performed to confirm that it represented a local minimum. The corresponding free energy barrier for the metathesis in solution

$$\underset{\mathbf{2}}{cis\text{-}[Rh(CO)_2I(CH_4)]} \rightarrow \underset{\mathbf{11}}{cis\text{-}[Rh(CO)_2(HI)(CH_3)]} \quad (8)$$

is $\Delta G_8 = 29.8$ kcal/mol.

The subsequent step in the mechanism is the exchange of HI for I^- in solution to produce the *cis*-$[Rh(CO)_2I(CH_3)]^-$ complex **3** (Figure 2g):

$$\underset{\mathbf{11}}{cis\text{-}[Rh(CO)_2(HI)(CH_3)]} + I^- \rightarrow \underset{\mathbf{3}}{cis\text{-}[Rh(CO)_2I(CH_3)]^-} + HI \quad (9)$$

This step is exoergonic with $\Delta G_9 = -13.0$ kcal/mol in solution. One can speculate that an intermediate concerted pathway for activation would possibly be very favorable. Such a mechanism was proposed[11] for the Periana system, where the ligand exchange of Cl^- for CH_4 takes place almost simultaneously with the C−H activation. That is, the dissociating Cl^- ligand takes on one of the hydrogens from methane and is eliminated as HCl. The analogous pathway in the case of the *cis*-$[Rh(CO)_2I_2]^-$ complex seems unfavorable, with an enthalpy of activation around 41.4 kcal/mol (in the gas phase). The geometry of the transition state is shown in Figure 2h.

C−H Activation by Oxidative Addition. The oxidative-addition mechanism is shown in Figure 3 for the most stable isomer of $[Rh(CO)_2I(CH_4)]$, *cis*-**2**. The *trans*-**2** conformation is less stable than *cis*-**2** by $\Delta G_{sol} = 13.8$ kcal/mol, due to the two CO ligands in trans positions. We have, however, investigated the oxidative process by *trans*-**2** as well, since a similar compound was reported[12] to have a low barrier for oxidative addition.

It follows from our calculations that oxidative addition to *trans*-**2** with a barrier of 9.7 kcal/mol in solution is more facile than oxidative addition to *cis*-**2**, for which the same barrier is 24.8 kcal/mol. The transition states for the cis and trans oxidative additions are shown in parts i and j of Figure 2, respectively. They have essentially the same values for the C−H bond length, the H−Rh−CH_3 angle, and the Rh−CH_3 distance. The overall activation is slightly more favorable for the trans isomer, for which the transition state has an energy of 23.5 kcal/mol relative to *cis*-**2.** While the transition states are very similar, the geometries of the products of the oxidative addition—compounds *cis*-**12** and *trans*-

(11) Kua, J.; Xu, X.; Periana, R. A.; Goddard, W. A. III. *Organometallics* **2002**, *21*, 511.
(12) Margl, P.; Ziegler, T.; Blchl, P. E. *J. Am. Chem. Soc.* **1995**, *117*, 12625.

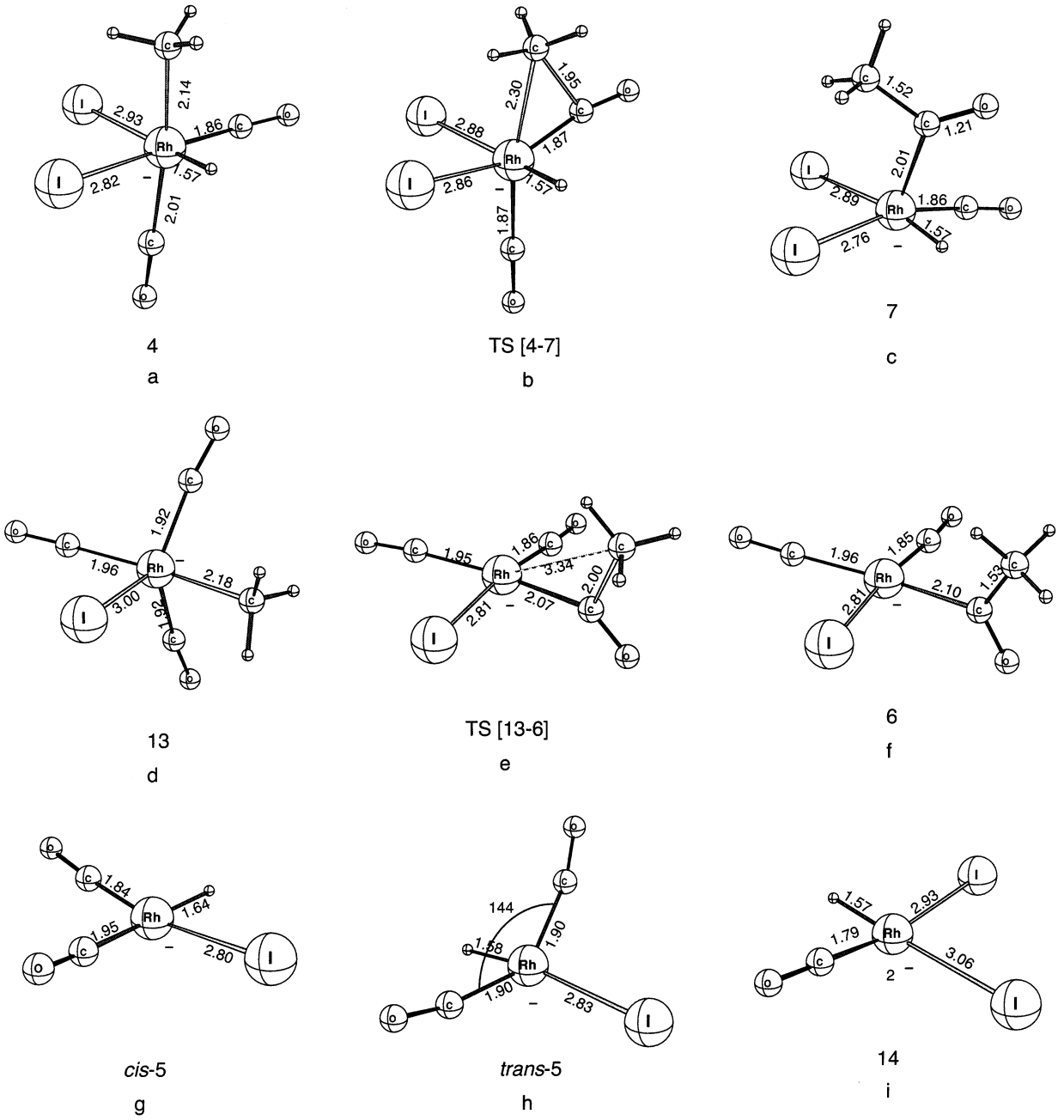

Figure 4. Optimized structures for the species involved in CO insertion and reductive elimination.

12—are very different, as shown in parts k and l, respectively, of Figure 2.

The cis isomer has a pyramidal structure, whereas the trans isomer is a deformed pyramid with a geometry not very different from that of the transition state itself. The overall free energy change in solution for the oxidative addition *cis*-$[Rh(CO)_2I(CH_4)] \rightarrow$ *cis*-$[Rh(CO)_2I(H)CH_3]$ (path **2** → **12** in Figure 3) is $\Delta G_{cis} = 20.8$ kcal/mol, compared to $\Delta G_{trans} = 7.2$ kcal/mol for the *trans*-**2** → *trans*-**12** path.

The oxidation state of Rh in the pyramidal complex **12** is 3, and it can add I^- in the vacant axial site to produce the hexagonal complex **4** (Figure 4a), or I^- can reductively eliminate the axial hydrogen to produce the square-planar $[Rh(CO)_2ICH_3]^-$ complex **3**. For the cis isomers the energies for the two steps

$$\underset{\textbf{12}}{cis\text{-}[Rh(CO)_2I(H)CH_3]} + I^- \rightarrow \underset{\textbf{4}}{cis\text{-}[Rh(CO)_2I_2(H)CH_3]^-} \quad (10)$$

$$\underset{\textbf{12}}{cis\text{-}[Rh(CO)_2I(H)CH_3]} + I^- \rightarrow \underset{\textbf{3}}{[Rh(CO)_2I(CH_3)]^-} + HI \quad (11)$$

are $\Delta G_{10} = 6.6$ kcal/mol and $\Delta G_{11} = -4.1$ kcal/mol, respectively, in solution. Thus, it would appear that the Rh(I) complex **3** is the most likely end product for the oxidative-addition path. The positive value for the iodide association in eq 10 is due to the strong solvation energy of I^-.

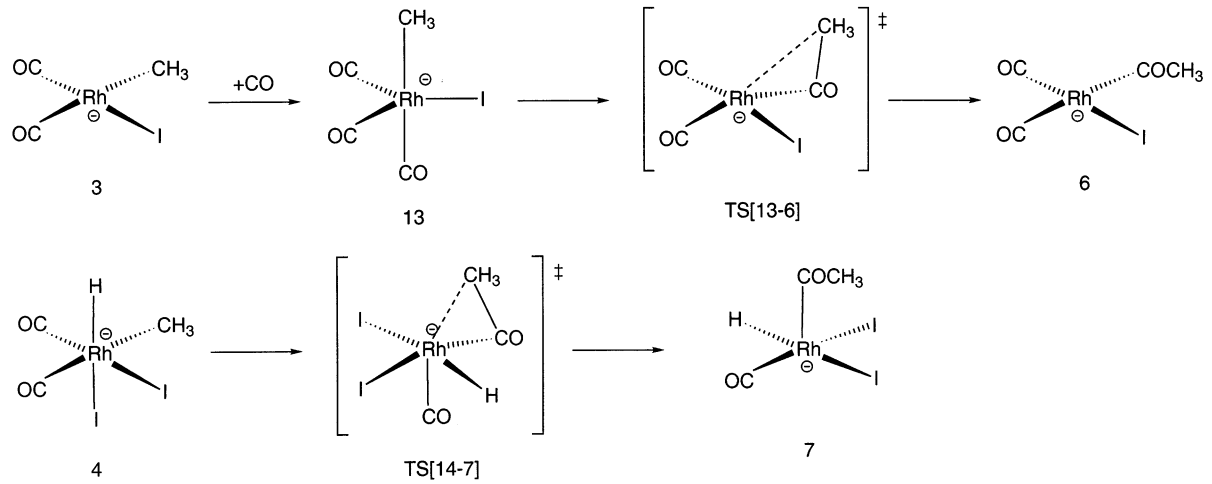

Figure 5. CO insertion mechanisms.

Scheme 2. Free Energy Profile for CO Insertion (kcal/mol)

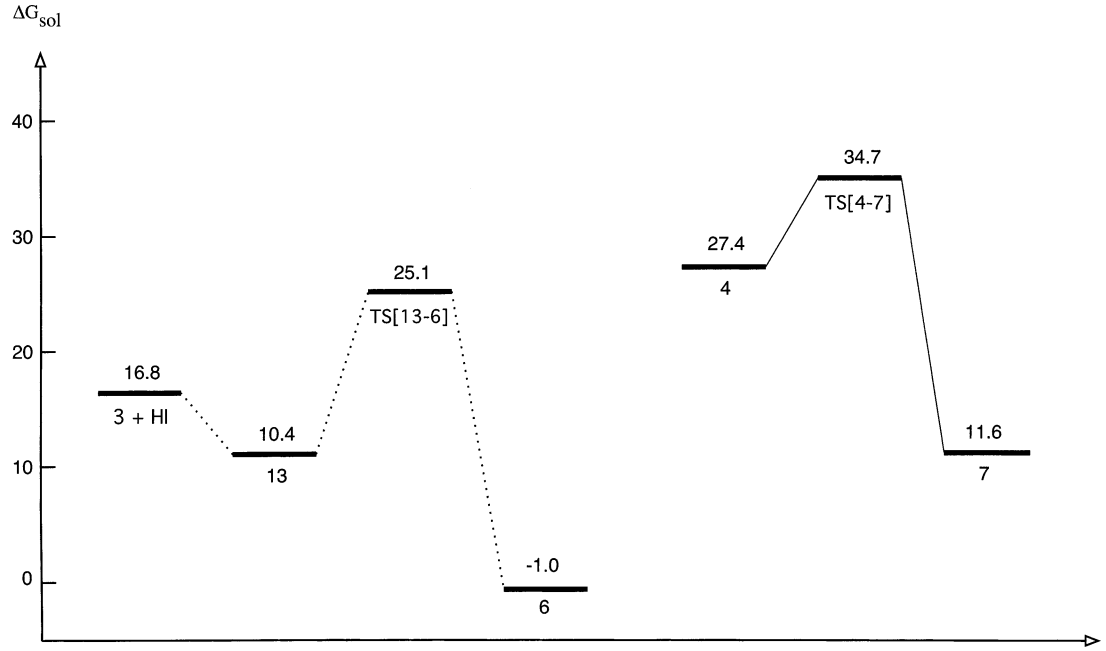

Table 3. Energies[a,b] for CO Insertion

reacn	ΔH_{gas}	ΔS_{gas}	ΔG_{gas}	ΔH_{sol}[c]	ΔS_{sol}	ΔG_{sol}
3 + CO → **6**	−21.2	−43.5	−5.6	−24.8	−19.8	−17.8
4 → **7**	−13.1	1.3	−13.5	−15.6	0.6	−15.8
4 → TS[**4-7**]	7.7	−2.0	8.4	7.0	−0.9	7.3
3 + CO → **13**	−11.6	−41.2	2.9	−13.0	−18.7	−6.4
13 → TS[**13-6**]	9.1	8.2	6.2	9.4	−14.9	14.7
13 → **6**	−9.6	−2.4	−8.8	−11.8	−1.1	−11.4

[a] See footnote *a* in Table 1. [b] See footnote *b* in Table 1. [c] See footnote *c* in Table 1.

The oxidative-addition mechanism is further seen to be favored over the metathesis mechanism because of the 6.3 kcal/mol lower barrier in the case of the trans oxidative addition (Scheme 1). Although the trans isomer of **2** is less stable, it provides for a lower barrier compared to the more stable *cis*-**2** isomer.

CO Insertion. The mechanisms we investigated for the CO insertion are shown in Figure 5. The energies for the CO insertion step are given in Table 3, with the energy profile shown in Scheme 2.

The CO insertion in the Monsanto reaction for carbonylation of methanol has been studied extensively. This process employs the same catalyst, **2**, as the Sen system. In the Monsanto case **2** oxidatively adds methyl iodide (formed by methanol and HI) to produce the hexagonal $[Rh(CO)_2I_3(CH_3)]^-$ complex. Kinetic studies demonstrate[13] that the subsequent carbonylation takes place through methyl group migration to one of the carbonyl ligands. An important role is played by the ligand trans to the methyl group, which can destabilize the $Rh-CH_3$ bond and assist the insertion. In this case the trans effect of the CO ligand is in part responsible for the low barrier of CO insertion, which we calculate to be around 7 kcal/mol. A similar methyl group migration to one of the carbonyl ligands takes place in a $Rh(PR_3)Cl(CO)$ complex generated[12] photolytically from $Rh(PR_3)Cl(CO)_2$.

(13) Cheong, M.; Schmid, R.; Ziegler, T. *Organometallics* **2000**, *19*, 1973.

For the Sen system we investigated the CO insertion in the square-planar complex **3** and the six-coordinated complex **4**, which are the two products of the C−H activation steps corresponding to the oxidative-addition mechanism and the metathesis pathways, respectively. For the migratory insertion involving the six-coordinated complex **4**

$$\underset{\mathbf{4}}{[Rh(CO)_2I_2H(CH_3)]^-} \rightarrow \underset{\mathbf{7}}{[RhCOI_2H(COCH_3)]^-} \quad (12)$$

we find the reaction free energy in solution to be $\Delta G_{12} = -15.8$ kcal/mol. The structure of the five-coordinated acyl compound **7** is shown in Figure 4c. It can be viewed as a square-pyramidal complex with the acyl group in the axial position. The insertion reaction (**4** → **7**) has a modest free energy of activation of 7.3 kcal/mol. The transition state TS[**4**-**7**] (Figure 4b) reveals that the methyl group slides parallel to the Rh−CO bond vector, while the local methyl C_3 axis rotates from a direction toward the metal to a direction toward the CO carbon. During the formation of the new acyl group the Rh−CO bond length is increased from 1.86 Å in complex **4** to 2.0 Å in complex **7**. As the CO carbon changes its hybridization, the Rh−C−O angle decreases gradually from 180° in complex **4** to 126° in complex **7**. Because of the acyl group's strong trans-directing effect, the most stable conformation of complex **7** has the acyl group in an axial position. As the carbonyl group leaves the plane of the complex to form the axial acyl group, the opposing CO ligand moves into the plane trans to the iodide ligands.

The second CO insertion path studied here involves complex **3** from the C−H activation along the metathesis pathway. For this planar system we considered a mechanism where an external CO is first associated to the complex to produce the stable $[Rh(CO)_3ICH_3]^-$ complex (compound **13** in Figure 4d) and then the CO insertion takes place. The initial CO addition is favorable in solution

$$\underset{\mathbf{3}}{[Rh(CO)_2ICH_3]^-} + CO \rightarrow \underset{\mathbf{13}}{[Rh(CO)_3ICH_3]^-} \quad (13)$$

with $\Delta G_{13} = -6.4$ kcal/mol. In the gas phase, where the entropy that is lost upon the CO addition is almost twice as great (around 41.2 cal/(mol K)), the addition is slightly uphill with $\Delta G_{13} = 2.9$ kcal/mol. Thus, under normal reaction conditions (high pressure of CO) we can expect **3** to be converted to **13** after the C−H activation along the metathesis pathway has taken place. For the migratory insertion by the second mechanism

$$\underset{\mathbf{13}}{[Rh(CO)_3ICH_3]^-} \rightarrow \underset{\mathbf{6}}{[Rh(CO)_2I(COCH_3)]^-} \quad (14)$$

$\Delta G_{14} = -11.4$ kcal/mol. The product of the insertion, complex **6**, is shown in Figure 4f. The transition state corresponds to the structure TS[**13**-**6**] (Figure 4e) with a free energy of activation of 14.7 kcal/mol.

The transition pathway here is very different from the one in the Rh(III) CO migration. The starting complex **13** is a trigonal bipyramid with one iodide and two carbonyl ligands forming the plane of the complex. The I−Rh−CO angle in this plane is 110°. The π-electron donation from the iodide to the carbonyls is not as effective as in the case of *cis*-**1**, for example, where the ligands are directly opposite each other. Hence, the bonds here are elongated. In TS[**13**-**6**] one can already observe the planar geometry of the end product—the methyl group has almost completely dissociated from the metal center, and the CO ligands have rearranged into a planar conformation. In complex **6** the Rh−$COCH_3$ and the Rh−CO_{trans} bonds are elongated because of the trans ligand effect of both the ligands. The transition state here is closer to the end product of the reaction than to the reagents.

The barrier that we obtained here for TS[**13**-**6**] is very close to both the theoretical and experimental values reported for the Monsanto process, despite the fact that in the **13** → **6** transition the metal center is in oxidation state I. This is due to the lack of a strong destabilizing ligand in the trans position in both cases. Surprisingly low, however, was the barrier for TS[**4**-**7**]. This transition state is structurally similar to the transition state for the $[Rh(CO)_3I_2(CH_3)]^-$ complex, for which an activation barrier of 12.7 kcal/mol has been predicted.[11] The substitution of one of the carbonyl groups (not trans to CH_3) by H leads to a barrier of only 7.3 kcal/mol (TS[**4**-**7**]). Such a low barrier could suggest that the CO insertion and migration is at least partially under diffusion control, due to the low solubility of CO (vide infra).

Reductive Elimination. The energies for the reductive elimination steps are given in Table 4, with the energy profile shown in Scheme 3.

The reductive elimination in the Monsanto process proceeds through acetyl iodide elimination. The experiments show this to take place through an unassisted internal elimination process. The process was also reversible. However, in the presence of nucleophiles such as acetate salts and secondary amines, an immediate and quantative reductive elimination takes place to produce acetic anhydride or the corresponding amide.[14] Therefore, for the Sen system we have investigated the nucleophilic attack mechanism. Further, we assume the barrier for this type of reaction to be small compared to the migratory insertion step, as has been found in the Monsanto process.

The reaction of the Rh−methyl (**4** of Figure 1) or −acyl (**7** of Figure 1) complexes with heptafluorobutyric acid results in the formation of the corresponding elimination products and a Rh(I)−hydrido complex (**5** in Figure 1). The elimination can in principle be carried out by H_2O as well, but given the high concentration of the acid and the high value for the acidity constant[15] $K_a = 1.1$, an elimination by the anion of the heptafluorobutyric acid via an S_N2 mechanism is more likely. An alternative mechanism for reductive elimination can be through a tricenter concerted elimination by the undissociated form of the acid. However, such a mechanism has been ruled out in a related Pt system, where an asymmetric carbon has been observed to change its stereochemistry upon reductive elimination.[16] It is expected that if a concerted mechanism were to come

(14) Maitlis, P. M.; Haynes, A.; Sunley, G. J.; Howard, M. J. *J. Chem. Soc., Dalton Trans.* **1996**, 2187.

(15) Hood, G. C.; Reilly, C. A. (Shell Development Co., Emeryville, CA) *J. Chem. Phys.* **1958**, *28*, 329.

Table 4. Energies[a,b] for Reductive Elimination

reacn	ΔH_{gas}	ΔS_{gas}	ΔG_{gas}	ΔH_{sol}[c]	ΔS_{sol}	ΔG_{sol}
3 + HA → *trans*-**5** + CH_3A	5.5	−0.2	5.5	6.8	−0.1	6.8
3 + A^- → **8** + CH_3A	114.9	−5.6	116.9	−20.1	−2.6	−19.2
4 + HA → *trans*-**5** + CH_3A + HI	20.5	37.2	7.4	2.1	16.9	−3.9
4 + A^- → *cis*-**5** + CH_3A + I^-	25.9	24.3	17.3	−67.7	10.9	−71.5
6 + HA → *trans*-**5** + CH_3COA	8.14	2.8	7.15	10.3	1.3	9.9
6 + A^- → **8** + CH_3CO-A	117.6	−2.6	118.5	−16.5	−1.2	−16.1
7 + HA + CO → *trans*-**5** + CH_3COA + HI	15.1	−4.5	16.6	−3.5	−2.1	−2.7
7 + A^- → **14** + CH_3COA	102.2	−5.0	103.9	−28.3	−2.3	−27.4

[a] See footnote *a* in Table 1. [b] See footnote *b* in Table 1. [c] See footnote *c* in Table 1.

Scheme 3. Free Energy Profile for Reductive Elimination (kcal/mol)

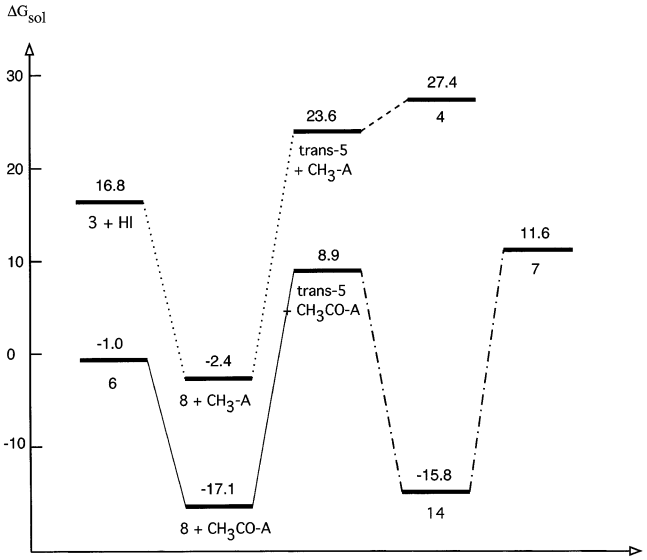

into play, then the product would retain the original stereochemistry of the carbon atom. The mechanisms we investigated for the reductive elimination are shown in Figure 6.

In the reductive elimination from the Rh(III)−methyl complex **4** by the anion of the acid, a simultaneous dissociation of one iodide ligand takes place, resulting in the direct formation of the Rh(I) compound **5**. The two possible isomers of the end product—complexes *cis*-**5** and *trans*-**5**, are shown in parts g and h of Figure 4, respectively. The trans form is found in solution to be only slightly more stable by $\Delta G_{sol} = -1.3$ kcal/mol. For the overall reaction with the undissociated form of the acid

$$\underset{\mathbf{4}}{[Rh(CO)_2I_2H(CH_3)]^-} + HA \rightarrow \underset{\mathbf{5}}{[Rh(CO)_2IH]^-} + HI + CH_3A \quad (15)$$

we get $\Delta G_{15} = -3.9$ kcal/mol for the trans product. In eq 15 HA is used to represent heptafluorobutyric acid, and CH_3A is the corresponding ester.

In the reductive elimination from the Rh(III)−acyl complex **7**, an intermediate $[RhCOI_2H]^{2-}$ complex was obtained (**14** in Figures 6 and 4i), which upon ligand substitution forms complex **5**. For complex **14** we found the cis isomer to be 17.2 kcal/mol more stable than the trans isomer on the enthalpic potential surface (ΔH_{sol}) in solution. This preference is in part due to the more favorable solvation energy of the cis conformer. For the reductive elimination from complex **7**

$$\underset{\mathbf{7}}{[RhCOI_2H(COCH_3)]^-} + A^- \rightarrow \underset{\mathbf{14}}{cis\text{-}[RhCOI_2H]^{2-}} + CH_3COA \quad (16)$$

we obtained $\Delta G_{16} = -27.4$ kcal/mol in solution. Here CH_3COA denotes the anhydride of acetic acid and heptafluorobutyric acid. For the overall reaction

$$\underset{\mathbf{7}}{[RhCOI_2H(COCH_3)]^-} + HA + CO \rightarrow \underset{\mathbf{5}}{[Rh(CO)_2IH]^-} + CH_3COA + HI \quad (17)$$

we get $\Delta G_{17} = -2.7$ kcal/mol in solution. In this investigation we are using a solvation method that will not account correctly for the specific interactions which are present in the system; therefore, instead of calculating ΔG for the ligand exchange reaction reaction **14** → **5** directly (where for consistency we consume the proton from the acid dissociation), we found it by subtracting ΔG(**7** → *trans*-**5**) and ΔG(**7** → **14**). In this manner one finds ΔG(**14** → *trans*-**5**) = 24.7 kcal/mol in solution. Therefore, the thermodynamic barrier one may expect for this process will be at least 24.7 kcal/mol and can be attributed to the considerable loss in the solvation energy and entropy of the reaction ions.

When the reductive elimination takes place from the Rh(I)−methyl and −acyl complexes, the oxidation state of the Rh atom will be reduced to −1, forming the complex shown in Figure 6 as **8**. The oxidation state of −1 has been known for Rh carbonyl compounds.[17] The geometry of this species is found in Figure 7a.

The structure of the complex is planar, with angles at the rhodium center close to 120°. The structure of this intermediate is very similar to that of the complex *trans*-**5**; hence, one can expect that the protonation of compound **8** will result in the trans isomer of complex **5**. Similarly, ΔG for the protonation reaction **8** → **5** can be found by subtracting ΔG(**3** → *trans*-**5**) and ΔG(**3** → **8**) (Table 4). Thus, one obtains ΔG(**8** → *trans*-**5**) = 26.0 kcal/mol in solution. This value will represent the thermodynamic barrier for the process and is again due to the considerable loss in the solvation energy and entropy of the reaction ions.

(16) (a) Luinstra, G. A.; Labinger, J. A.; Bercaw, J. E. *J. Am. Chem. Soc.* **1993**, *115*, 3004. (b) Luinstra, G. A.; Wang, L.; Stahl, S. S.; Labinger, J. A.; Bercaw, J. E. *J. Organomet. Chem.* **1995**, *504*, 75.

(17) Deblon, S.; Rüegger, H.; Schnberg, H.; Loss, S.; Gramlich, V.; Grützmacher, H. *New J. Chem.* **2001**, 25, 83.

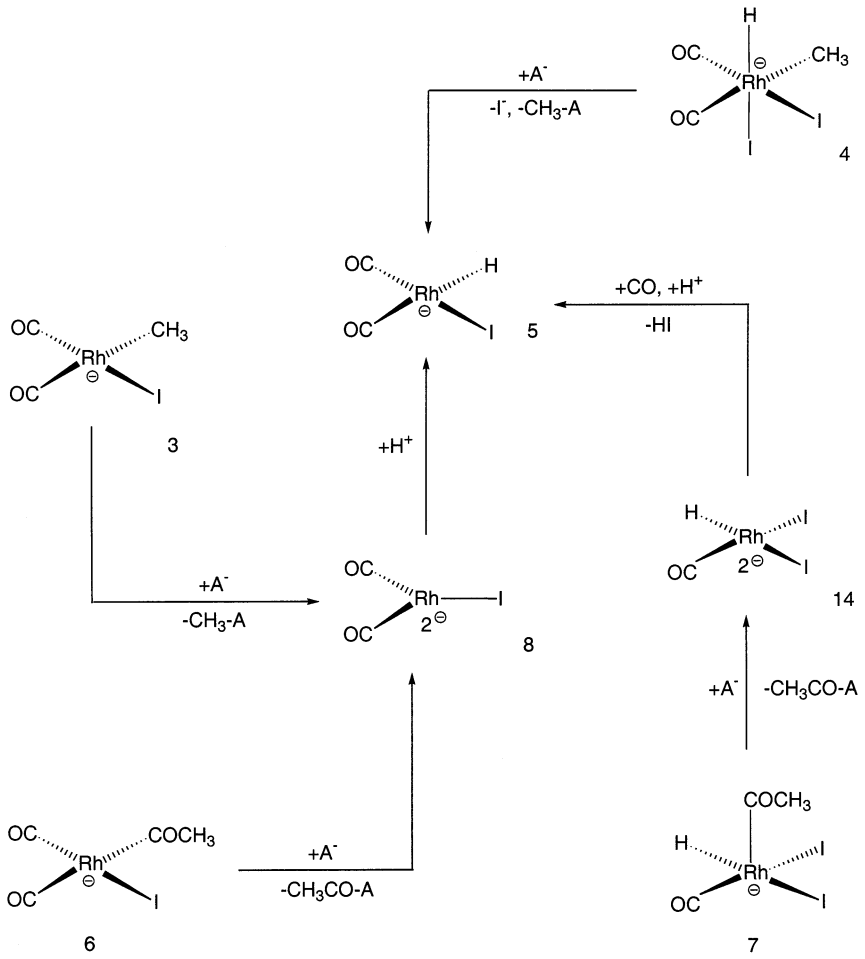

Figure 6. Proposed mechanisms for the reductive-elimination step.

In summary, the more favorable elimination reactions are with the Rh−acyl complexes. These findings confirm the product ratio observed by Sen in low heptafluorobutyric acid concentrations, where the acetic acid (in the form of the anhydride) was the dominating product. However, in the case of high acid concentrations the selectivity switches to methanol. It can be expected that a very low solubility of CO in heptafluorobutyric acid can account for this finding. While there are no experimental data for heptafluorobutyric acid, the solubility in trifluoroacetic acid is prohibitively low.[18] On the other hand, as the concentration of the acid increases, the elimination reaction starts to compete with the CO insertion process, thus resulting in an increased formation of methanol. In support of this qualitative argument is the fact that upon addition of methanol to the acid system, which leads to esterification of the acid and an increased solubility of CO, the selectivity was reversed back to acetic acid.

Oxidation. The mechanisms we propose for the oxidation of the metal hydride *cis*-**5** are shown in Figure 8. The energies for the oxidation steps are given in Table 5, with the energy profile shown in Scheme 4.

Dioxygen has been known to insert into metal−hydrogen bonds for Co, Rh, Ir, and Pt complexes.[19] For instance, in the presence of base a Rh(I) complex was oxidized[20] to the corresponding hydroperoxo complex by O_2. In the proposed mechanism an OH^- group first reduces the starting Rh^{III}−H complex to a more reactive Rh(I) complex, which upon oxygen uptake and subsequent protonation produces a Rh^{III}−OOH complex. It was observed that at higher concentrations a reaction of the type

$$Rh^{III}-H + Rh^{III}-OOH \rightarrow 2Rh^{III}-OH \qquad (18)$$

can also take place and is faster than the dioxygen insertion. The rate of the oxidation was high in the presence of base, whereas for low pH values the reaction was slow.

Table 5. Energies[a,b] for Metal Hydride Oxidation

reacn	ΔH_{gas}	ΔS_{gas}	ΔG_{gas}	ΔH_{sol}[c]	ΔS_{sol}	ΔG_{sol}
cis-**5** + O_2 → **9**	−34.7	−36.4	−21.8	−50.5	−16.5	−44.7
9 → TS[**9**-**10**]	12.0	0.4	11.9	15.5	0.2	15.4
9 → **10**	−25.9	3.1	−26.9	−27.1	1.4	−27.6
10 + I^- → *cis*-**1** + OOH^-	35.6	10.6	31.9	34.6	4.9	32.9
10 + *cis*-**5** → **25**	−71.5	−4.4	−69.9	−74.6	−2.0	−73.9
15 + I^- → *cis*-**1** + OH^-	48.5	7.6	45.8	37.3	3.5	36.1
10 → **16** + OH^-	77.6	28.7	67.4	29.2	12.9	24.6

[a] See footnote *a* in Table 1. [b] See footnote *b* in Table 1. [c] See footnote *c* in Table 1.

(18) Fujioka, G. S.; Cady, G. H. *J. Am. Chem. Soc.* **1957**, *79*, 2451.
(19) See references cited in ref 21.
(20) Gillard, R. D.; Heaton, B. T.; Vaughan, D. H. *J. Chem. Soc. A* **1970**, 3126.

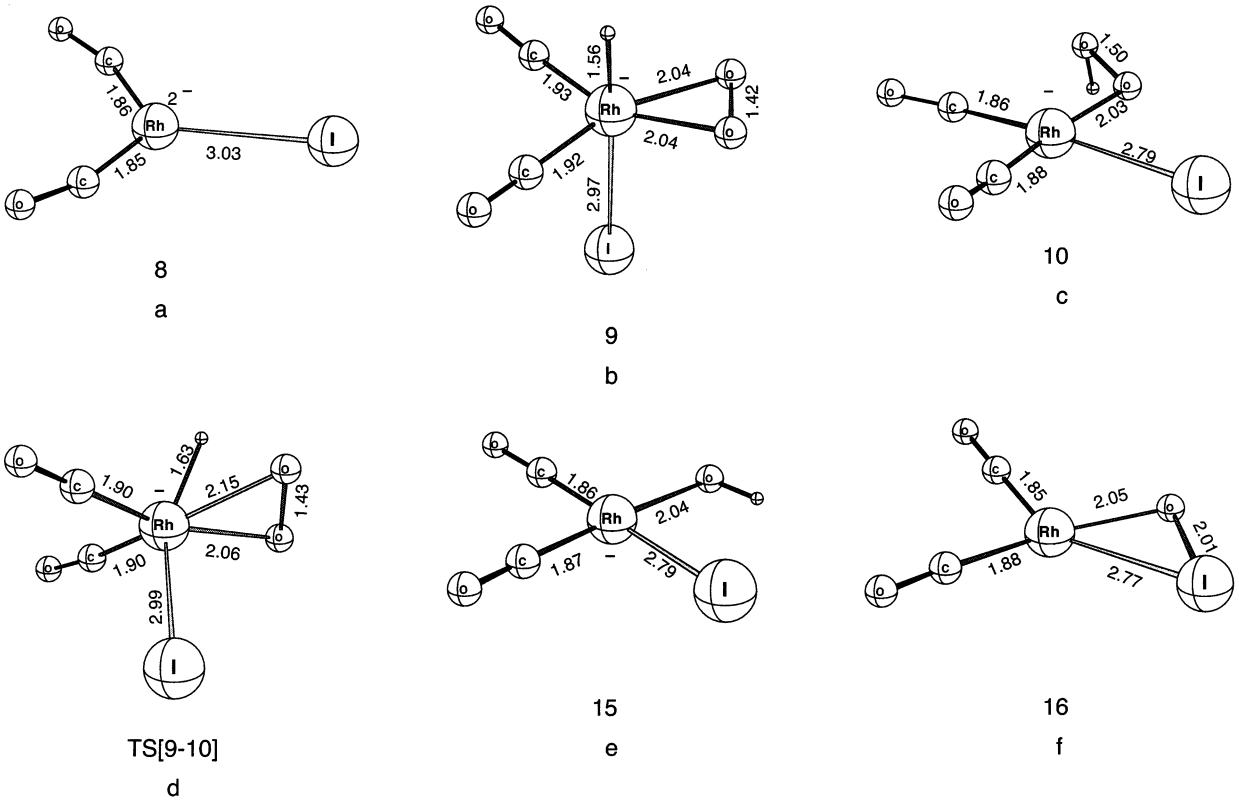

Figure 7. Optimized structures for the species involved in reductive elimination and oxidation of Rh−H species.

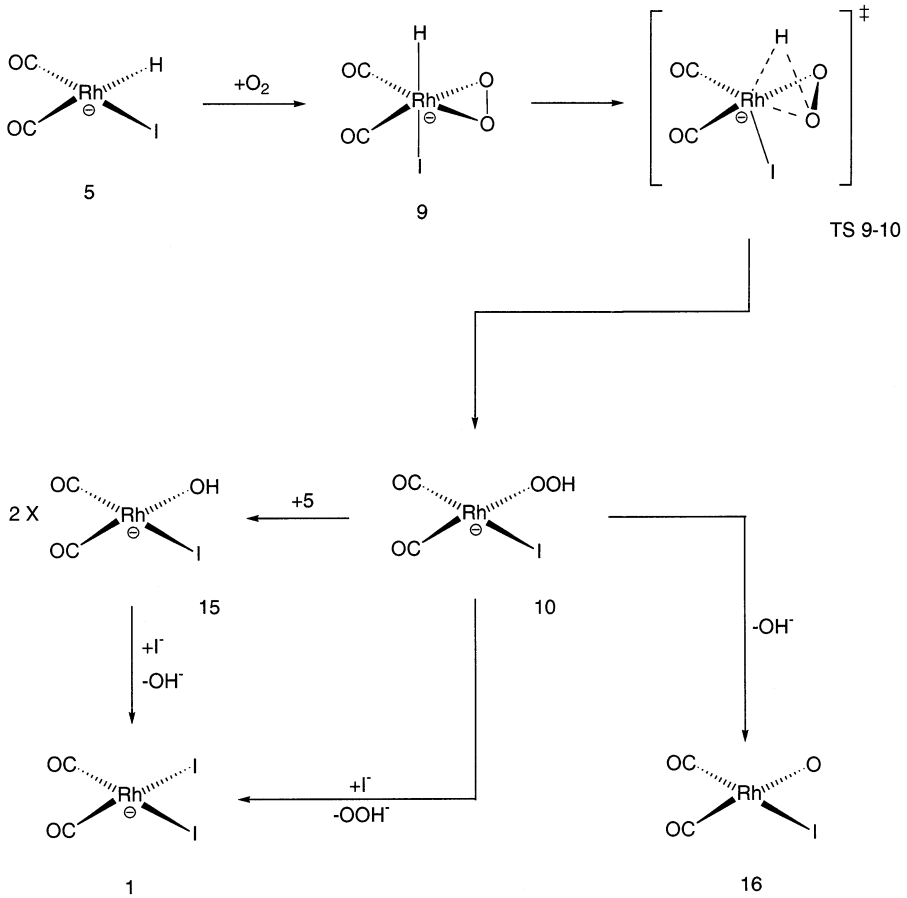

Figure 8. Proposed mechanisms for the oxidation step.

Recently it was discovered[21] that Pt^{IV}−H complexes can also insert O_2 in the absence of base. In this case a more likely mechanism for the initial deprotonation is through a hydrogen radical abstraction. Upon thermoly-

Scheme 4. Free Energy Profile for Oxidation (kcal/mol)

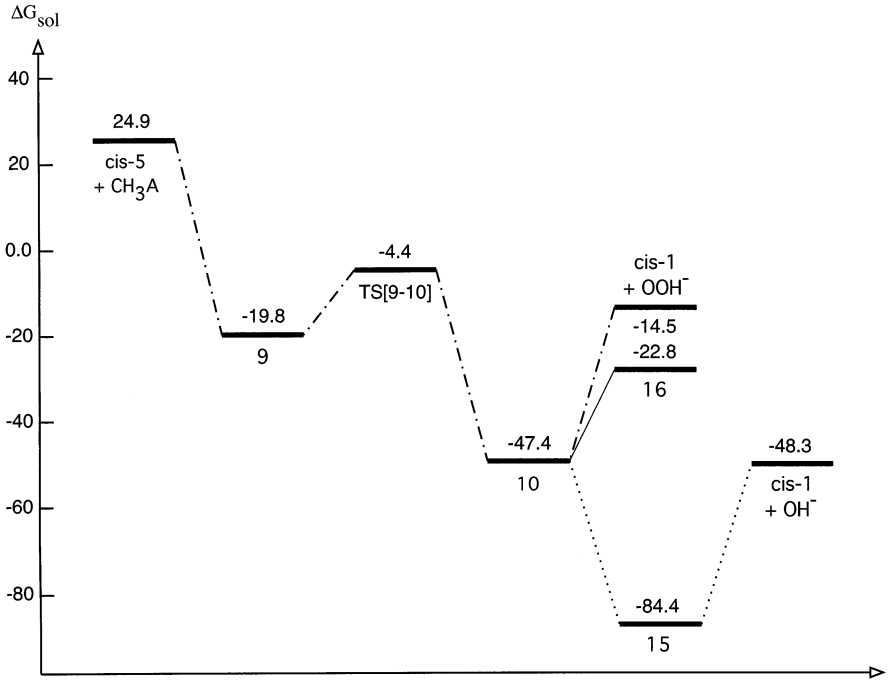

sis the hydroperoxo complex produced a hydroxo complex, thus suggesting that a process similar to that shown in eq 18 can take place in organic solvents.

In the proposed mechanism dioxygen will first associate to *cis*-**5** to form the η_2-O_2 complex **9** (Figure 7b):

$$\underset{\mathbf{5}}{cis\text{-}[Rh(CO)_2IH]^-} + O_2 \rightarrow \underset{\mathbf{9}}{[O_2Rh(CO)_2IH]^-} \quad (19)$$

This process is highly exoergonic, with $\Delta G_{19} = -44.7$ kcal/mol in solution. The protonation of the peroxo group can be achieved by an external proton as well as by migration of the hydride ligand. The barrier for the intramolecular protonation is 15.4 kcal/mol and corresponds to transition complex TS[**9**-**10**], shown in Figure 7d. In the acidic medium one can expect an even lower barrier for the process if the proton source is the solvent. Thermodynamically the reaction is also very favorable:

$$\underset{\mathbf{9}}{[O_2Rh(CO)_2IH]^-} \rightarrow \underset{\mathbf{10}}{[(HOO)Rh(CO)_2I]^-} \quad (20)$$

with $\Delta G_{20} = -27.6$ kcal/mol in solution. The geometry of the product, complex **10**, is shown in Figure 7c.

Once the peroxo group is formed, there are several possible mechanisms for its transformation. Complex **10** could react with the hydrido complex **5** to produce 2 equiv of the hydroxo complex **15**:

$$\underset{\mathbf{10}}{[(HOO)Rh(CO)_2I]^-} + \underset{\mathbf{5}}{[Rh(CO)_2IH]^-} \rightarrow 2\underset{\mathbf{15}}{[(HO)Rh(CO)_2I]^-} \quad (21)$$

Such a transformation has been seen experimentally in a similar Rh complex.[20] This process is extremely favorable, with $\Delta G_{21} = -73.9$ kcal/mol in solution. The geometry of complex **15** is shown in Figure 7e. Upon ligand exchange the hydroxy group in **15** is substituted with iodide to produce the catalyst complex **1**:

$$\underset{\mathbf{15}}{[(HO)Rh(CO)_2I]^-} + I^- \rightarrow \underset{\mathbf{1}}{[Rh(CO)_2I_2]^-} + OH^- \quad (22)$$

For this step we obtained $\Delta G_{22} = 36.1$ kcal/mol in solution.

A far less favorable alternative is the dissociation of the peroxo group in complex **10** to oxygen and OH^- to produce complex **16**:

$$\underset{\mathbf{10}}{[(HOO)Rh(CO)_2I]^-} \rightarrow \underset{\mathbf{16}}{[Rh(CO)_2OI]} + OH^- \quad (23)$$

For this step we obtained $\Delta G_{23} = 24.6$ kcal/mol in solution. The geometry of complex **16** can be seen in Figure 7f. The structure and bond lengths in that complex point toward a bidentate hypoiodite group being formed. We have not investigated the chemistry of that complex any further, since a large number of possible transformations can take place. If the hypoiodite group can be dissociated as such, it may also be reasonable to suggest a CH_4 functionalization by OI^-, which has been observed in oleum,[22] in the absence of metal catalyst.

On the basis of the thermodynamic evidence it seems even less likely to have a direct ligand exchange of the peroxo group in complex **10** with iodide to produce complex **1**:

$$\underset{\mathbf{10}}{[(HOO)Rh(CO)_2I]^-} + I^- \rightarrow \underset{\mathbf{1}}{[Rh(CO)_2I_2]^-} + OOH^- \quad (24)$$

for which we obtain $\Delta G_{24} = 32.9$ kcal/mol in solution. Even though this process seems to be the most endo-

(21) Wick, D. D.; Goldberg, K. I. *J. Am. Chem. Soc.* **1999**, *121*, 11900.

(22) See U.S. Patent 6,380,444.

ergonic one, one has to keep in mind that after another catalytic cycle the hydrido species will be oxidized once again, where as in the case of the two nuclear reactions between complexes **10** and **5**, the energy obtained corresponds to the oxidation of 2 equiv of the hydrido complex **5**. There is some indirect evidence that oxidation could take place beyond the metal center. In the labeling experiments of Sen methanol did not produce acetic acid (which would be expected if a $Rh-CH_3$ complex formed) but was oxidized to HCOOH. Our assertion is that if the peroxo group were to dissociate into the solution, it could oxidize methanol to formic acid.

Conclusion

The catalyst used in the Sen system readily exchanges ligands to allow for methane to enter into its first coordination sphere. The C−H activation proceeds with a relatively low barrier for the oxidative-addition mechanism, which is preferred over the metathesis mechanism. A CO insertion step similar to that in the Monsanto system leads to the formation of Rh−acyl species. The rate of the CO insertion and reductive elimination govern the selectivity of the process. In low acid concentrations the dominating product is acetic acid, whereas for higher acid concentration the major product is methanol. The oxidation by O_2 is facile via a Rh−peroxo complex.

Acknowledgment. This research was supported by funding from the NSERC and the University of Calgary. T.Z. wishes to thank the Canadian government for a Canada research chair in theoretical inorganic chemistry.

Supporting Information Available: Tables giving the optimized geometries of the structures discussed (Cartesian coordinates, in Å). This material is available free of charge via the Internet at http://pubs.acs.org.

OM030217C